Numerical Approach on Hybrid PID-AFC Controller using Different Intelligent Tuning Methods to Reduce the Vibration of the Suspended Handle

Mohd Hafiz Abdul Satar, Wong Jen Nyap and Ahmad Zhafran Ahmad Mazlan

School of Mechanical Engineering, Universiti Sains Malaysia, Engineering Campus, 14300, Nibong Tebal, Penang, Malaysia.

(Received 9 May 2020; accepted 9 November 2020)

This paper focusses on the study of vibration attenuations for suspended handle models that are generated from power tools using an intelligent active force control (AFC) tuning strategy. Four types of control schemes are comparatively evaluated in suppressing the vibration of the handle, such as proportional-integral-derivative (PID), PID-AFC-crude approximation (AFCCA), PID-AFC-fuzzy logic (AFCFL) and PID-AFC-iterative learning method (AFCILM) control schemes. In all control schemes, the estimated counter force is generated from the actuating force and appropriate estimated mass (M^*) that has been intelligently tuned to counter the system disturbances. The disturbances are modelled based on the power tools vibration (i.e., internal disturbance) and uncertainties during the operation (i.e., external disturbances). The study shows that the AFCCA scheme demonstrates the best performance when the M^*_{CA} is tuned at 0.04 kg. For the AFCFL control scheme, the best response is obtained for the membership function of trapezoidal shape with M^*_{FL} of 0.0403 kg, while for AFCILM control scheme, the best response is achieved when M^*_{ILM} is tuned to 0.04 kg, with both parameters (A and B) set at 0.6. Overall, PID-AFCCA scheme shows the best performances for all of the case studies, followed by PID-AFCFL and PID-AFCILM. The findings of this study can benefit the power tool manufacturers and provide the basis of effectively intelligent controller design for the power tools application.

1. INTRODUCTION

Vibration is undesirable in most cases, whereby it can cause failure or damage to the systems and produce hazardous effects to humans. Hand-arm vibration syndrome (HAVs) is an example of a common health issue caused by the use of hand-held power tools that operate at low frequencies with high levels of vibration.[1] The effect of prolonged and unregulated use of these tools will cause the vibration to propagate to the whole human body system including the shoulder, back, neck and head.[2–5] The worst case, one with a large magnitude of vibrations, or shocks for example, might cause harm to the soft and hard tissues of the joint structures.[6,7] Therefore, researchers have introduced several control methods. These control methods are generally known as passive and active vibration controls (AVC). The passive control involves the use of reactive or resistive devices that either load the transmission path of the disturbing vibration or absorb the vibration energy.[8] Shunt dampings,[9] shunted piezo-ceramics,[10] and dynamic absorbers,[11] are examples of isolation devices that are used to dissipate the vibration. However, for the dynamic system where the disturbance is varying over time, passive vibration control becomes inefficient,[12] wherein an AVC system must be introduced. AVC is a system with an active power source that can control and attenuate the vibration in real-time, by providing counterforce in opposite phase but equal in amplitude to the source of vibration.[13,14]

In the literature, different types of AVC controllers have been developed to obtain the required level of counter vibration signal. The proportional-integral-derivative (PID) is one of the effective controllers that has been widely used in the AVC system. It consists of three principal control parameters, such as proportional (P), integral (I), and derivative (D) gains. Each parameter has its function, and any combination of these three parameters will produce the desired controller output.[15] Carbajal et al.[16,17] proposed a dynamic feedback tracking control using a PI controller for the synchronous motors. From the studies, the uncertain dynamic load was able to suppress and provided better performance with smooth motion profiles. Regards to different combination of P, I, and D parameters, Jovanovič et al.[18] reported that the PID controller could reduce the vibration level up to 94.82 %, followed by PD (94.31 %), PI (93.94 %) and P (93.6 %) control schemes. Zhang et al.[19] also suggested that PID controller as a better control method compared to D, PD, and linear quadratic regulator. Thus, the PID became a preferable controller and has been utilized in different kinds of applications such as DC motors,[20] automotive,[21] and air flight control.[22]

Another effective controller used for vibration regulation is called active force control (AFC). This controller operates by computing the estimated disturbance force via actuator force and mass acceleration which is subjected to an appropriate tuning of the estimated mass. The simple diagram and the low computational time makes it an attractive option in real-time control applications.[23,24] An example of the tuning method in AFC involves using fuzzy logic (FL). Mailah and Rahim[1] proposed an AFCFL method for a rigid robot arm. This intelligent method was compared with a basic PD scheme to investigate

the trajectory track performance of the rigid robot arm. The findings show that the PD scheme has a large track error of up to $10\ mm$ while, in contrast, the AFCFL scheme shows lower error of $0.7\ mm$. Rao et al.[25] investigated the effectiveness of the FL controller to deal with uncertain vibration parameters i.e., road surfaces. Based on the investigation, the FL controller was found to be suitable to reduce the vibration level and enhance the performance of the car suspension system. In similar application, Nizar et al.[26] improved the control scheme with the combination of sliding mode neural network inference FL controller, to deal with the nonlinearity of the car suspension as well as the parameters of uncertain vibrations. The outcome shows that the FL controller reduces the vibration level and improved the ride and comfortability level. Continuous evaluation of this control scheme was conducted to reduce the vibration generated by friction-induced from the sliding surfaces. Positive results reported by Dehkordi et al.[27] from the series of tests and proved that the AFCFL is more effective when compared to the PID controller.

Crude approximation (CA) is one of the AFC control tuning schemes. The first implementation of AFCCA on the suspension car system was performed by Peng et al.[28] Subsequently, Gohari et al.[29] had expanded the work by proposing the neuro-AFCCA control scheme on the seat suspension system. The study reported severe displacement of the seat pan and human body parts (i.e., body and head) and by implementing the control scheme, it was able to attenuate the undesirable vibrations effectively. Meanwhile, Abdullah et al.[30] analysed the control scheme with the feedforward model to eliminate the disturbances in the motion control of a mobile manipulator. This control scheme was also used by Mazlan et al.[31] to reduce the disturbances on the sander-arm system. The PD and AFCCA control schemes were investigated and it was found that PD increased the transmitted vibration to the system, while, for the system using the AFCCA scheme, a linearly decreasing trend of vibration was achieved. Another study conducted by Hassan et al.[32] to evaluate the PID and AFCCA control schemes for the rear handle of the hedge trimmer and the finding also showed that the AFCCA has effectively reduced the disturbances.

The Iterative learning method (ILM) was developed by Arimoto et al.[33] to challenge the current control scheme and was the least reported among all the AFC control schemes. Jian et al.[34] implied the ILM control scheme for the direct inverse of hysteresis to mitigate the nonlinearities of the system. The control scheme was further evaluated by Xu et al.[35] on the precise motion tracking, which agreed with Jian et al., such that ILM can utilize both the input and output data and overcome the limitations of the feedback algorithm. On the other hand, Kwek et al.[24] considered the PD, AFCCA, AFCILM control schemes on the biped robot application. The error obtained by AFCILM was larger by only 1.7 % as compared to AFCCA for all the cases when the initial setting was incompatible. The AFCILM was tested without prior knowledge of the system, which was an interesting feature of the controller. Other schemes such as AFCCA were used with the prior knowledge of the system but was impractical for most of the cases. Huang et al.[36] optimized this method on human-powered augmentation lower exoskeletons and the result showed that the control strategy could handle the changing interaction dynamically, as compared to conventional augmentation method.

From the literature, numerical approach seemed to offer a promising result of the study at a low-cost, by providing better visualization with the ability to solve complex problems. Several numerical approaches have been selected for the development of a model such as smart material characterization,[37] non-linear actuator characterization,[38] and energy harvester.[39] Nevertheless, this approach has also been implied for different types of AVC systems. Mazlan et al.[40] compared the performance of the AFCCA and the AFCFL for reducing the vibration of the suspended handle. In the research work by Purnomo et al.,[41] the PID, AFCCA, and AFCFL control schemes were compared in the application of liquid container transport. The control scheme was used to suppress liquid sloshing. In a closed study, Hassan et al. compared the AFCCA, AFCILM, and AFCFL with a PID control scheme, but in a different application i.e. hedge trimmer. All the reported control schemes had varying performance measures and the nature of variation depending on the applications. Nevertheless, it is clear that the applications involving AFC control schemes are not abundantly available in the literature. Although Mazlan et al.[40] conducted a study on the use of different schemes for reducing the vibration for the suspended handle, there is a need to explore the potential of combining all the control schemes available to attenuate vibration for the same application.

In this study, the numerical approach was employed as it was important to understand the influence of different control schemes, prior to the real-time hardware-based experimentation. The fundamental controller for all control schemes was the PID control and acted as a benchmark for the AFC control scheme. The proposed AFC control schemes to be investigated are PID-AFCCA, PID-AFCFL, and PID-AFCILM controllers. For the membership function (MF) in the AFCFL control scheme, trapezoidal,[41–43] triangular,[27,44,45] and generalized bell shape[25,46,47] functions were included as successful variations were reported on these functions. The effectiveness of the control schemes and the passive system were simulated and evaluated using Simulink/MATLAB software.

2. METHODOLOGY

2.1. System Modelling

The model used in this study was based on the active suspended handle developed in previous studies.[29,30,48] The model was centred on the single degree of freedom (DOF) system, which consisted of components such as dynamic mass (m), stiffness (k), and damping (c) as shown in Fig. 1. The *m*, *c* and *k* values were determined from the frequency response function (FRF) of the experimental modal analysis (EMA).[49] The AVC system was modelled by adding a counterforce (F_a) from the piezoelectric actuator to compensate the disturbance force (F_s).

The equation of motion for the AVC system is shown in Eq. (1). The actuator force, F_a value was generated through the PID controller and different intelligent AFC schemes.

$$m\ddot{x}\,(t) + c\dot{x}\,(t) + kx\,(t) = F_s(t) - F_a(t); \qquad (1)$$

where $F_s = F_1$ and F_2.

There were two types of disturbances that had been introduced to the system, namely internal (F_1) and external (F_2)

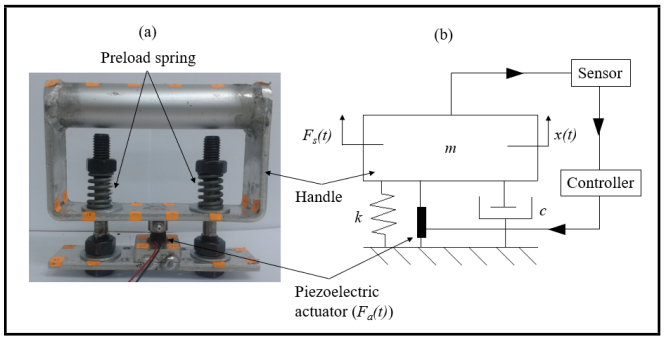

Figure 1. (a) Actual and (b) model of the suspended handle.[48]

Table 1. The dynamic mass, stiffness, and damping for the passive system.

Parameter	Value
Dynamic mass, m (kg)	0.04
Dynamic stiffness, k (Nm^{-1})	33.45
Dynamic damping, c (kgs^{-1})	3.78×10^5

disturbances. The internal disturbance was based on the input disturbance from the vibration tool, according to a previous study.[31] The internal disturbance model was a sine wave signal with an amplitude (F_0) and excitation frequency (ω) of 20 N and 200 Hz, respectively. In this study, the external disturbances that had been introduced were represented by the external forces implied to the system. These disturbances were only introduced to the system after the tuning process of the controllers in order to investigate the robustness of the AVC system.

For external disturbances, there were two different types, namely external disturbances A and B. External disturbance A was represented as the non-linear effect of the hard stop from the environment during the operation of power tools,[12,24] while for B, it represented the non-linear effect of imbalance motor at different frequencies.[50] These disturbances were represented using the following equations:

$$F_{2A} = F_0 \sin\omega(t) F_{\mathrm{HS}}; \tag{2}$$

$$F_{2B} = F_{01} \sin\omega_1(t) + F_{02} \sin\omega_2(t); \tag{3}$$

where F_{2A} and F_{HS} were the external disturbance A and blocking amplitude of the hard stop, respectively. Meanwhile, F_{2B} was the external disturbance B, wherein ω_1 and ω_2 were the frequency functions of the imbalance corresponding to the first and second motor orders, respectively. F_{01} and F_{02} represented the amplitudes of both imbalance frequencies. With regard of DOF used in this study, Tang and Yang,[51] and Xiao et al.[52] have extended works on multiple DOF by adding masses and piezoelectric actuators for the systems.

The system was firstly modelled without the feedback control loop to provide the passive corrective action to the disturbances. Generally, without the active feedback control action, the system generated a poor response and deviated from the targeted reference input. In this system, the parameters m, c, and k were obtained from the FRF results based on a previous study[49] and presented as in Tab. 1.

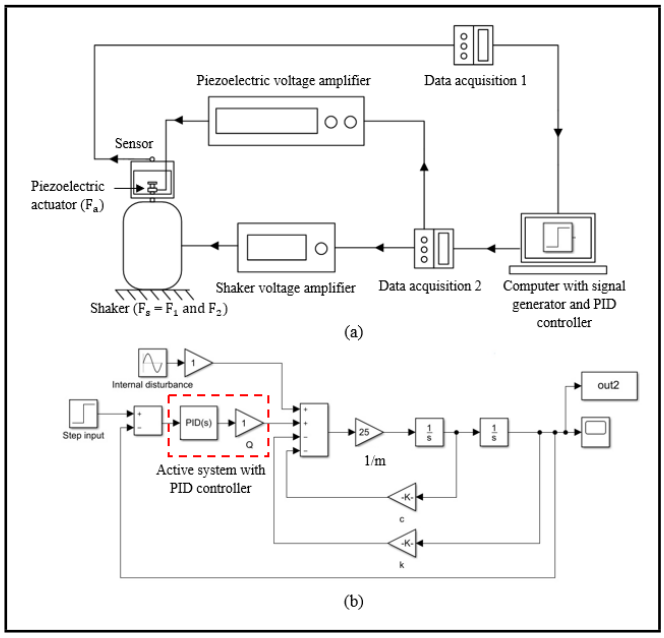

Figure 2. (a) Schematic and (b) block diagrams for the AVC system with PID controller.

2.2. AVC System with PID, AFCCA, AFCFL and AFCILM Schemes

Figure 2 illustrates the schematic diagram for the possible experimental setup and block diagram of the AVC system with a PID controller. The input force (i.e., disturbance) was excited by the shaker where it exerted F_1 and F_2 to the suspended handle and caused the structure to vibrate harmonically, as in Eq. (2) and (3). A piezoelectric was mounted on the suspended handle to provide the counter force (F_a) based on the PID controller, as shown in Fig. 2(a). The piezoelectric actuator and shaker were connected to a data acquisition and voltage amplifier to receive and amplify the signals, respectively. In this study, the actuator gain (Q) value was set as $1\frac{N}{m}$ to generate maximum force from the PID controller, which was based on the study by Mann et al.[53] The theoretical PID controller equation is given in Eq. (4). The resultant vibration between the piezoelectric actuator and shaker was measured by a sensor and connected to another data acquisition to transfer the acquired data to the data acquisition software.

$$u_c(t) = K_P e(t) + K_I \int_0^t e(t')\,dt' + K_D \frac{de(t)}{\mathrm{dt}}. \tag{4}$$

In this study, four types of AVC schemes, namely PID, PID-AFCCA, PID-AFCFL, and PID-AFCILM, were investigated to attain the desired output values numerically. In the Simulink software, the block diagram of the AVC system was developed as shown in Fig. 2(b). Additionally, PID controller in Fig. 2(b) acted as the base controller for all the AFC systems. On the other hand, the system had a feedback control loop to calculate the error signal in the passive system.

In the PID-AFFCA system, the disturbance force was attenuated with the addition of estimated disturbance force (F^*) of the AFC controller, which is based on Eq. (5).

$$F^*(t) = F_a(t) - M^* \ddot{x}(t); \tag{5}$$

where F_a was the force from the actuator, M^* was the estimated mass and $\ddot{x}$ was the mass acceleration of the handle.

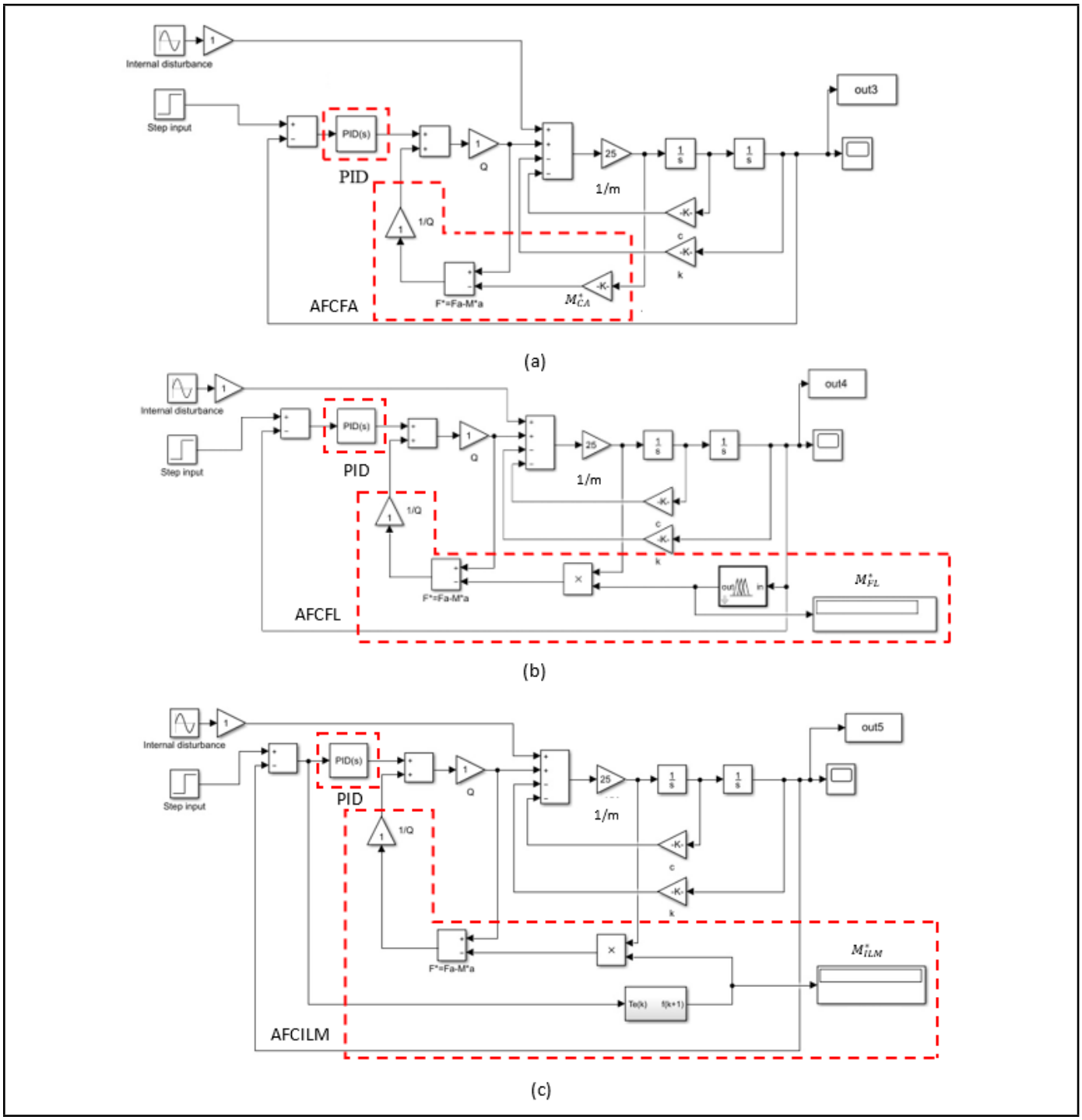

Figure 3. Block diagram of the AVC system with (a) PID-AFCCA, (b) PID-AFCFL and PID-AFCILM controllers.

The block diagram of the AVC system with PID-AFFCA is shown in Fig. 3(a), where the estimated disturbance force was determined from M^*_{CA}. The estimated disturbance force (F^*) was multiplied with the inverse gain of actuator $(1/Q)$ before it was added to the total counter force of the system. The M^*_{CA} was tuned manually with the different approximated values (crude approximation) until the desired output was obtained.

For the AFCFL scheme in Fig. 3(b), the M^*_{FL} value was carefully tuned as it might result in a more accurate estimated mass value. This scheme used the FL controller, which consisted of three main steps, namely (1) fuzzification, (2) execution of rules, and (3) defuzzification of the system.[54] The significance of these three steps was centred on the implementation of the input range value, process input value through pre-set membership function (MF), and lastly, the approximation of output value. In this case, the input and output values were represented by the targeted mass displacement range (y_{out}) and M^*_{FL} as shown in Fig. 4(a) and 4(b), respectively.

The range of both values was determined based on the results of mass displacement and M^*in the previous PID-AFCCA scheme which was set between $4.9 \times 10^{-6}\ m\ to\ 6.2 \times 10^{-6}$ m and $0.02\ kg\ to\ 0.06\ kg$, respectively. As shown in Fig. 3(b), the mass displacement signal was taken as an input range value to the FL block as in FL editor command panel in Fig. 4(a) and the FL algorithm processed the values using

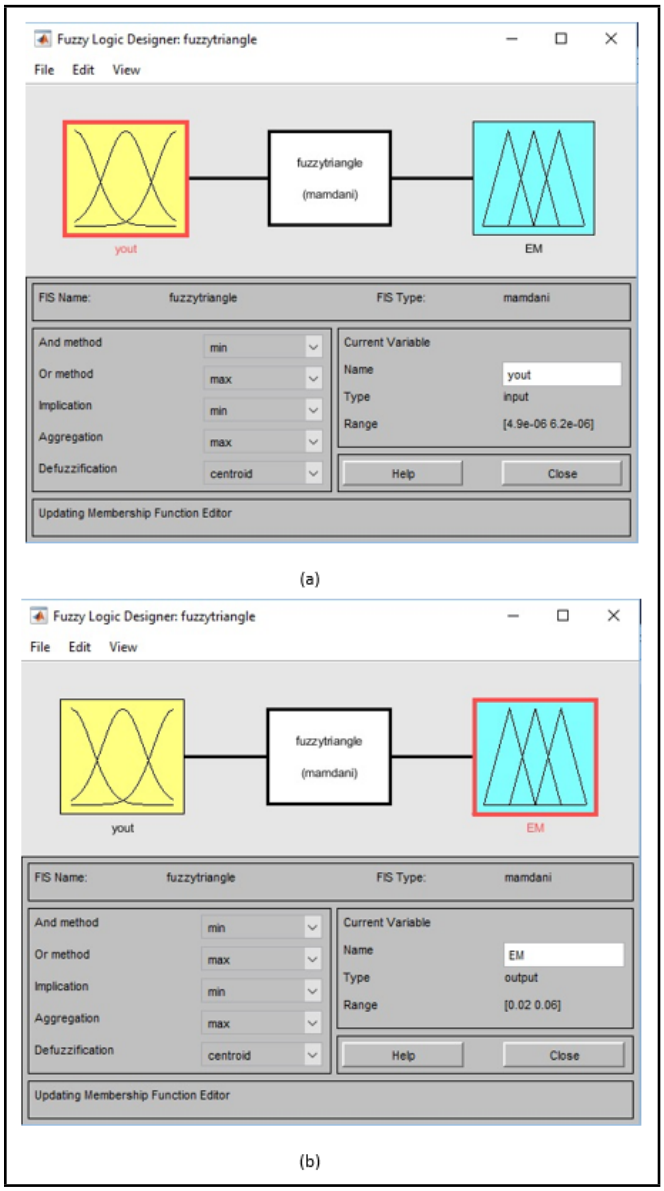

Figure 4. FL editor command panel for (a) input range and (b) output range.

three type of MF, including triangular, trapezoidal, and generalized bell shape functions. Then, the FL generated the most optimum M^*_{FL} value based on the output estimated mass range set in Fig. 4(b).

For the AFCILM scheme, there was an addition of initial mass (IM) and learning parameters A and B to the Simulink block diagram as shown in Fig. 3(c). The equation for the ILM is presented as follows:

$$M_{\mathrm{ILM}}{}^{*k+1} = M_{\mathrm{ILM}}{}^{*k} + \left(A + B\frac{d}{\mathrm{dt}}\right) Te_k; \qquad (6)$$

where $M_{\mathrm{ILM}}{}^{*k+1}$ was the next step value of the M^*, $M_{\mathrm{ILM}}{}^{*k}$ was the current step value of the IM, A, and B were proportional and derivative parameters, respectively and Te_k was the current track error. The Te_k can be further explained as following equation:

$$\mathrm{Te}_k\,(t) = \; y_d\,(t) - y_k\,(t)\,; \qquad (7)$$

where, Te_k was the difference between the desired output (y_d) and the current output (y_k) of the system. With the $M_{\mathrm{ILM}}{}^{*k+1}$ in the system, the repeated response of the system was able to supress the error to the best solution value. The error converged as the iteration number increased.[32] For the tuning of ILM parameters, the IM was set at an optimum mass value that was obtained from PID-AFCCA, previously. Similarly, the learning parameters A and B were then tuned until the best performance of the controller was obtained.

Table 2. Parameters of the tuned PID controller.

Controller parameter	Coefficient value
Proportional gain (K_p)	1.281×10^7
Integral gain (K_I)	2.056×10^9
Derivative gain (K_D)	1.842×10^3
Filter coefficient (N)	5.322×10^6

Table 3. M^*_{FL} values generated from the FL controller using different MF.

MF	$\mathrm{M}^*_{\mathrm{FL}}$, kg
Triangular shape	0.04039
Trapezoidal shape	0.04029
Generalized bell shape	0.04042

2.3. Performance Analysis of the Controllers

In this study, the step input signal analysis was conducted to determine the best performance among the PID and hybrid PID-AFC schemes. In this analysis, the values of targeted output and step size were set at 5×10^{-6} m and 0.01 s, respectively. This step value was retrieved from a previous study,[55] where the values corresponded to the maximum displacement of the piezoelectric actuator. Other parameters such as the vibration overshoot, rise time, and settling time of the system with and without external disturbances were also investigated and analysed to determine the best controller for the system.

3. RESULTS AND DISCUSSION

3.1. Passive System and AVC with PID Scheme

The desired output response is mainly controlled by the gains of the PID controller, as formulated in Eq. (8). Figure 5(a) shows the output response of the system before (i.e. block response) and after (i.e. tuned response) the tuning of the PID controller based on the set target output. The result shows that the tuned response has less overshoot and a better settling time. Tab. 2 highlights the values of K_P, K_I, K_D and the filter coefficient parameter (N) that were automatically generated using the PID auto-tuning method provided in the Simulink software. The PID auto-tuning method is used here to target the balance output in terms of performance and robustness which includes the closed-loop stability, rapid disturbance suppression and the enough margin for the variation of the system dynamics. The N is the coefficient that used to implement the derivative action. The values obtained were then implied in the PID controller of the AVC system.

Figure 5 shows the responses of the passive and AVC system with a PID controller in the time domain. For the passive system, the internal disturbance is firstly introduced, as stated before in Section 2.1. The first peak of the displacement has the highest displacement value of 7.6×10^{-5} m and then attained steady state with an amplitude range in between

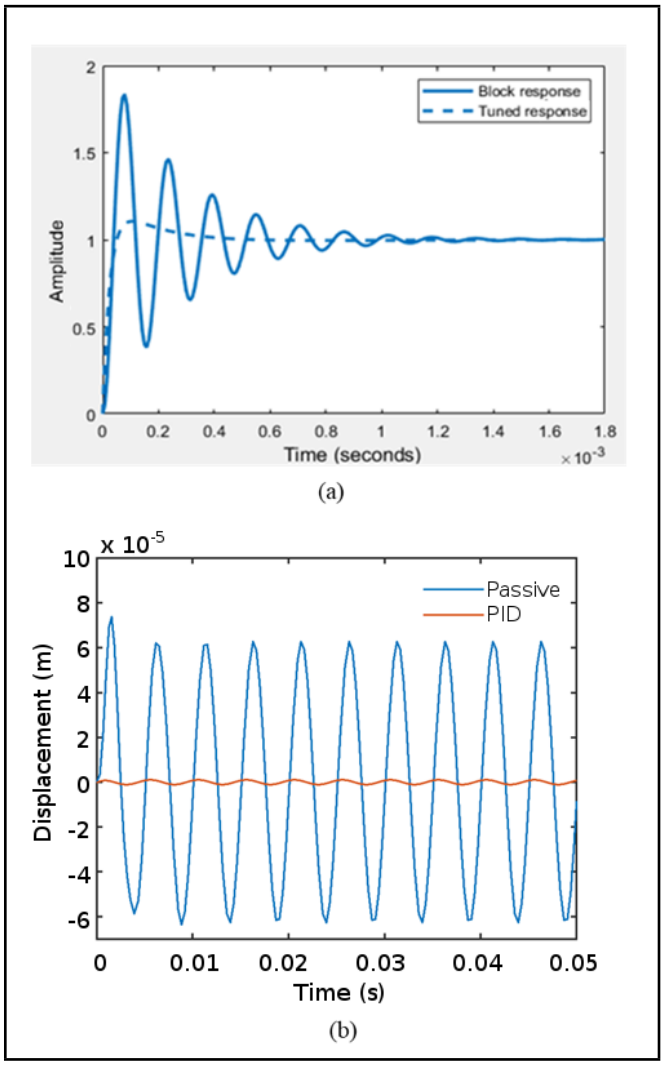

Figure 5. Responses comparison for (a) PID tuning block and (b) passive and AVC with PID controller.

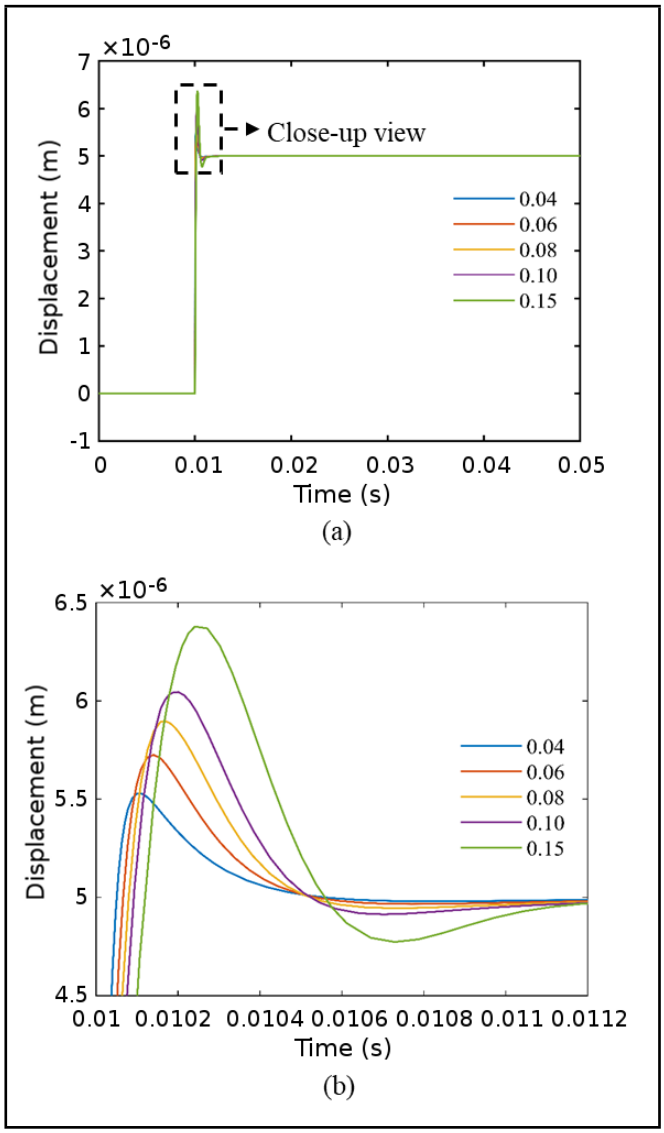

Figure 6. (a) Overall and (b) close-up views of mass displacement for different M^*_{CA} in PID-AFCCA controller.

$\pm$ 6 $\times 10^{-5}$ m until 0.05 s of time. In the case of applying AVC with PID controller, the highest output displacement reduced to $\pm$ 1 $\times 10^{-5}$ m, which showed a significant vibration reduction for the system.

$$U_c(s) = K_p - K_I \frac{1}{s} + K_D \frac{N}{1 + N\frac{1}{s}}. \quad (8)$$

3.2. AVC System with PID-AFCCA Scheme

For the PID-AFCCA system, the tuned PID controller in Section 3.1 was added with the AFC algorithm using the estimated mass, *M**. The system output response was investigated for different values of M^*_{CA} (i.e. 0.04 kg, 0.06 kg, 0.08 kg, 0.1 kg and 0.15 kg). An internal disturbance and step input with a target value of 5 $\times 10^{-6}$ m is introduced to the AVC system, whereby, this value was taken from the previous study.[49]

Figure 6(a) and (b) show the results of the output displacement for different M^*_{CA} values for PID-AFCCA controller. From the figures, it can be noticed that the best response is obtained for M^*_{CA} value of 0.04 kg, whereby, the least overshoot and shortest settling time is obtained compared to other M^*_{CA} values. The trend also indicates that, with an increase in M^*_{CA} values, the output displacement exhibits a larger overshoot and begins to oscillate. Meanwhile, when the value of M^*_{CA} was reduced below than 0.04 kg, the overshoot became poor even though the settling time was reduced. Thus, M^*_{CA} values that are larger or lower than 0.04 kg tend to show an undesirable output response and may not be applicable to the current system. This finding is compatible with the results reported by Mazlan et al.[40], wherein the optimized *M** value was like the dynamic mass value of the system (i.e. 0.04 kg) and the result gave the best response for the output displacement. There are some case studies that obtained different *M** values compared to the dynamic mass values due the non-linearity of the models.[31,32]

3.3. AVC System with PID-AFCFL Scheme

In this section, the results of output displacement for the PID-AFCFL controller using different types of membership functions (MF) are presented. Tab. 3 shows the M^*_{FL} values that are generated using different MF shapes of the FL scheme. From the table, the generalized bell shape has the highest M^*_{FL} value of 0.04042 kg, followed by triangular and trapezoidal shapes.

Figure 7 (a) and (b) show the results of output displacement for three different types of MF for the PID-AFCFL con-

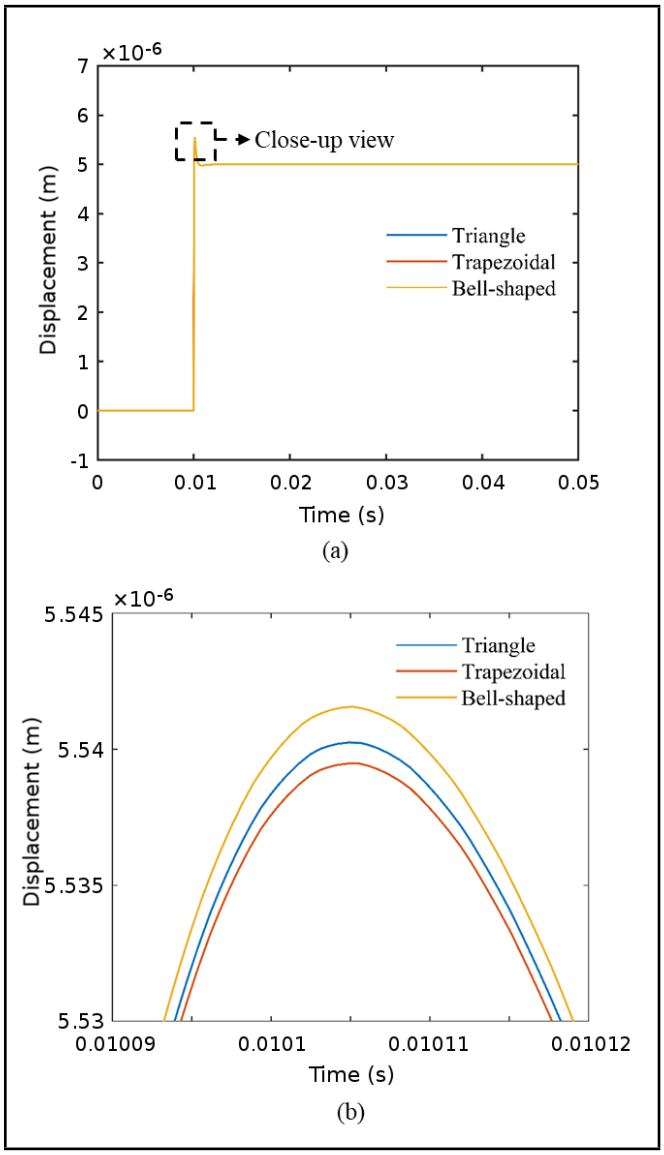

Figure 7. (a) Overall and (b) close-up views of output mass displacement for different MFs.

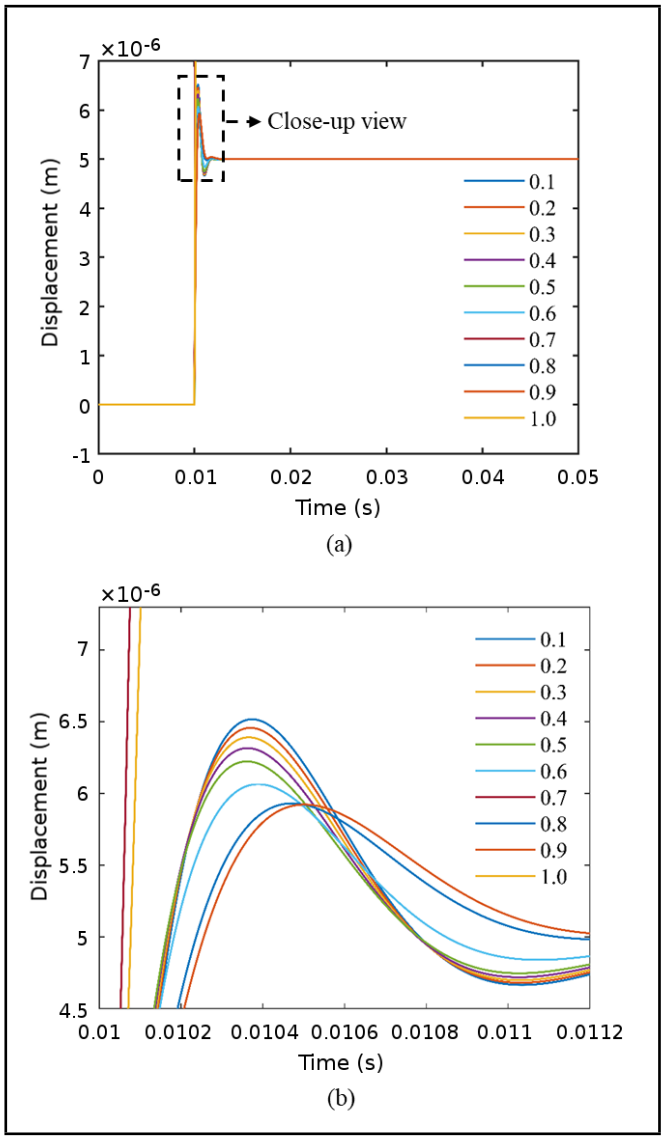

Figure 8. (a) Overall and (b) close-up views of output displacement response for different parameter values of A and B.

troller. From the figure, it can be observed that the trend for all three MFs has a closely similar pattern of output displacement. However, in the magnified view (Fig. 7 (b)), which provides a detailed comparison, the trapezoidal shape presents the best performance when compared to the triangular and generalized bell shapes. The order of the displacement response is in coherence with the generated M^*_{FL} values, in which the best performance is noticed for M^*_{FL} value close to 0.04 kg (trapezoidal shape = 0.04029 kg). Thus, further analysis for the AFCFL controller is performed using trapezoidal shape MF.

3.4. AVC System with PID-AFCILM Scheme

Iterative learning method (ILM) is made up of algorithms with an initial value and learning parameters (i.e., A and B). For example, at first, the initial value was taken as 0.04 kg, which was the optimum M^* value obtained in the previous analysis (Section 3.1). Then, the learning parameters A and B are tuned with different values to determine the better output response. In this study, both A and B values were set with the same range of 0.1 to 1.0 with an interval of 0.1 in the presence of internal disturbance and step input.

Figures 8 (a) and (b) shows the result of output displacement for PID-AFCILM with an initial value of 0.04 kg and different A and B values. From the figures, the discrepancy was observed when the learning parameters A and B were set at 0.7 and 1.0, respectively. At this condition, the output displacement becomes unstable, and increases tremendously, as shown in the magnified view in Fig. 8 (b). At the peak region, the output displacement response exhibited a distinct performance compared to other values of parameters A and B, as shown in Fig. 8 (b). The best learning parameter values for both A and B are found at 0.6, wherein it shows an enhanced overall performance in terms of overshoot, rise, and settling times. Below 0.6, the displacement curves exhibit a higher rise time and poor overshoot. On the contrary, for values above 0.6, the displacement curve had lower overshoot but longer settling time.

The AFCILM scheme is investigated for different learning parameter values of A and B. Tab. 4 summarizes the result of M^*_{ILM} values for different A and B values. The M^*_{ILM} values in the table indicate that the learning parameter values become unstable in response and deviate from the targeted signal, which is more than -3000 kg for both the values of A (0.7) and B (1.0). While for other parameters, the value is almost close

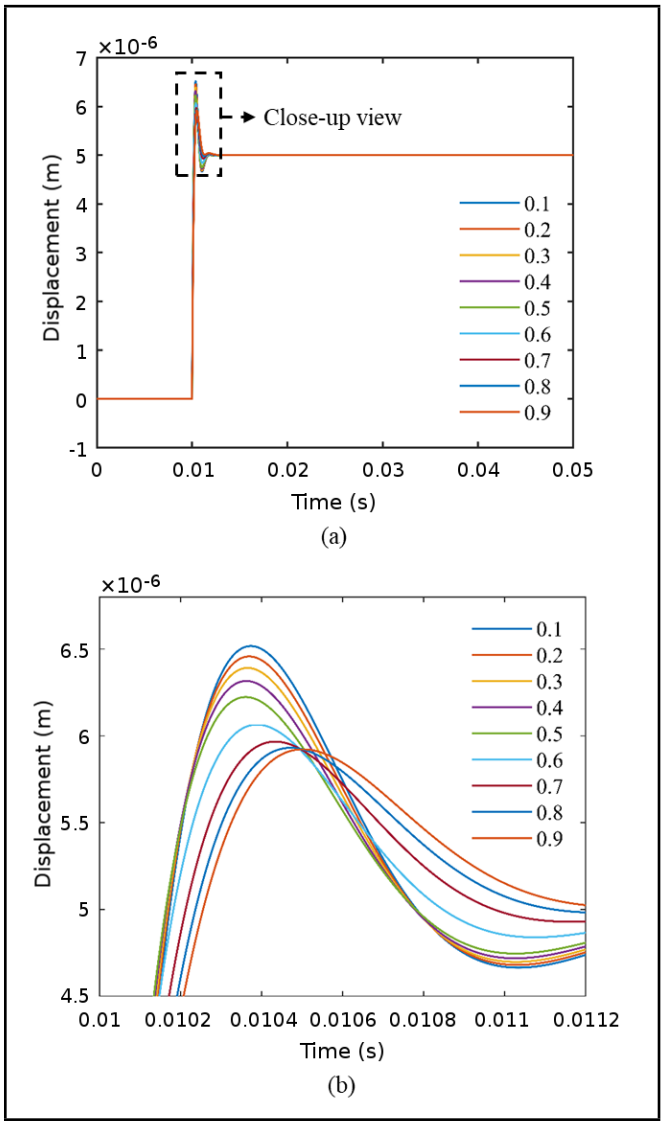

Figure 9. (a) Overall and (b) close-up views of output displacement response with parameter A = 0.6.

to 0.04 kg and had desired output displacement responses.

The parameter values of A and B are then manipulated to study the effect of fixing one parameter at a constant value (A or B) at 0.6. Figure 9 shows the output displacement response for a fixed parameter value (A = 0.6) with a changing parameter B, and for a reversal of the same phenomenon, is shown in Fig. 10.

For a fixed value of parameter, A (Fig. 9), the output response displacement has a similar trend as obtained previously in Fig. 8 (parameters A and B are equal to 0.6), and this combination is maintained for parameter B = 0.6. But a different trend is observed when parameter B was fixed (Fig. 10), wherein the output displacement showed differences for different parameter values of A except for 0.2, 0.3, 0.5, 0.7, and 0.9. The responses tend to deviate from the desired output and become unstable, which highlights that parameter A determines the stability of the system. In overall, the best performance of AFCLIM is achieved when the estimated mass value M^*_{ILM}, parameters A and B are set at 0.04 kg, 0.6, and 0.6, respectively. The values of A and B for the ILM controller are difficult to be predicted since it is based on the mathematical model developed. Study by Kwek et al.[24] show that the different values of

Table 4. M^* values for different A and B values.

A and B values	M^*_{ILM}, kg
0.1	0.0399
0.2	0.0400
0.3	0.0399
0.4	0.0400
0.5	0.0399
0.6	0.0400
0.7	-3019.9
0.8	0.0399
0.9	0.0399
1.0	-3016.8

Table 5. Combinations of different disturbances analysis.

Step input signal
Internal disturbance only
Internal + External disturbance A
Internal + External disturbance B

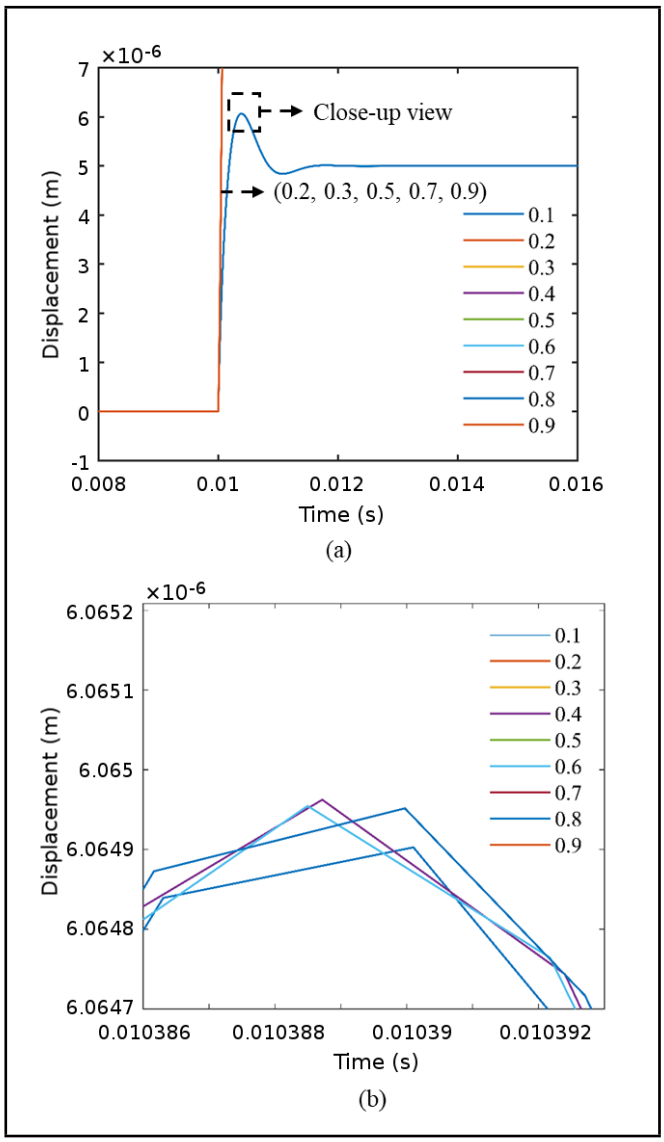

Figure 10. (a) Overall and close-up views of output displacement response with parameter B = 0.6.

learning gain parameters were determined for the 5-link biped robot.

3.5. Performance Analysis

In this section, all the controller systems were tested using the step input signal and the combination of both internal and external disturbances as summarized in Tab. 5.

Figure 11 (a) – (c) shows the output mass displacement of the step input signal with internal disturbance. From the figures, it is observed that the step input signal was not affected by the passive system since the vibration amplitude is larger than the set step value itself. However, the AFC schemes show good responses in achieving the target value of 5×10^{-6} m compared to the passive and PID systems. From this study, AFCCA produced the best performance for the step input signal, followed closely by AFCFL. The AFCILM somehow showed poor performance among all the AFC schemes in terms of overshoot, rise, and settling times.

The output displacement responses of all the systems added with the external disturbance A are shown in Fig. 12 (a) – (c). Like Fig. 11, the AFFCA shows the best performance, followed by AFCFL and AFCILM schemes. Also, the output response from the PID controller was subjected to the same oscillation along with the target step value of 5×10^{-6} m in the presence of external disturbance A. Thus, the latter controller was found to be less effective for the current system.

Figure 13 (a) – (c) shows the output displacement response of all the systems when the external disturbance A is replaced with B. The figure shows that the passive and PID systems were affected by the replacement of external disturbance B, similar to that of findings reported by Hassan et al.[32] Meanwhile, all the AFC schemes achieved the target value in countering the vibration and were capable of adapting the change in the disturbance (i.e., disturbance A and B). On comparing the AFC schemes, the AFCCA scheme shows a better performance for the output response, followed by the AFCFL and the AFCILM. For each of the disturbances that are introduced in Fig. 11, 12 and 13, all the AFC schemes faced similar difficulties to maintain the robustness of the controller by not affecting the targeted output displacement. However, all the schemes are effective even under the influence of various disturbances and conditions. This is due to the addition of estimated disturbance force (F^*) to the system with continuous feedback sensing from the actuator force and mass acceleration, as shown in the AFC block diagrams in Fig. 3.

Tab. 6 summarizes the comparison between all the AFC schemes. From the table, the optimum M^* values for the PID-AFCCA, PID-AFCFL and PID-AFCILM are obtained at 0.04 kg, 0.0403 kg and 0.04 kg, respectively and these values produce the best AVC performance for the suspended handle application. With the best M^* value, the targeted displacement peak values slightly differ for all the AFC schemes and the PID-AFCCA has produced the lowest value at 5.5×10^{-6} m. This peak displacement of the PID-AFCCA is close enough with the target displacement of 5×10^{-6} m. For the overall performances using the step input signal, the PID-AFCCA scheme exhibited an upper hand over other schemes as it demonstrated the best response with the lowest overshoot (i.e., 5.53×10^{-6}), fastest rise time and shortest settling time for the AVC system.

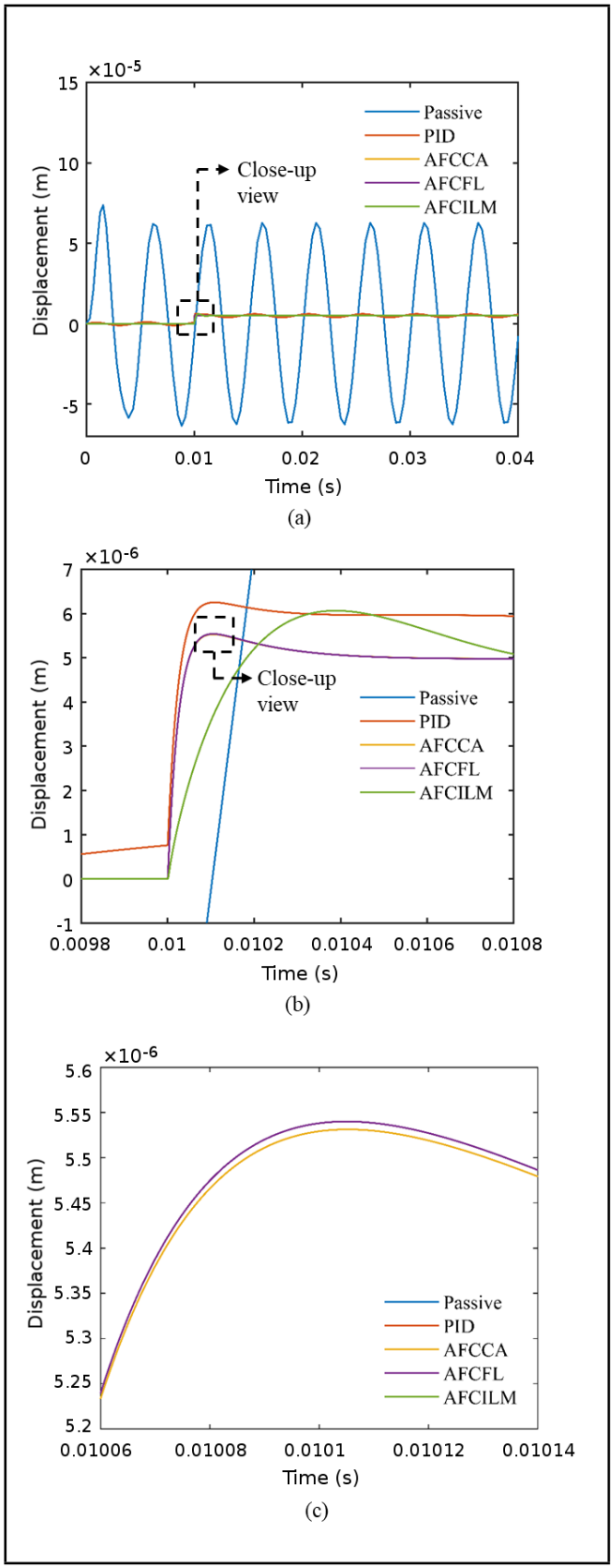

Figure 11. (a) Overall, (b) first level and (c) second-level close-up views of output displacement of step input with internal disturbance.

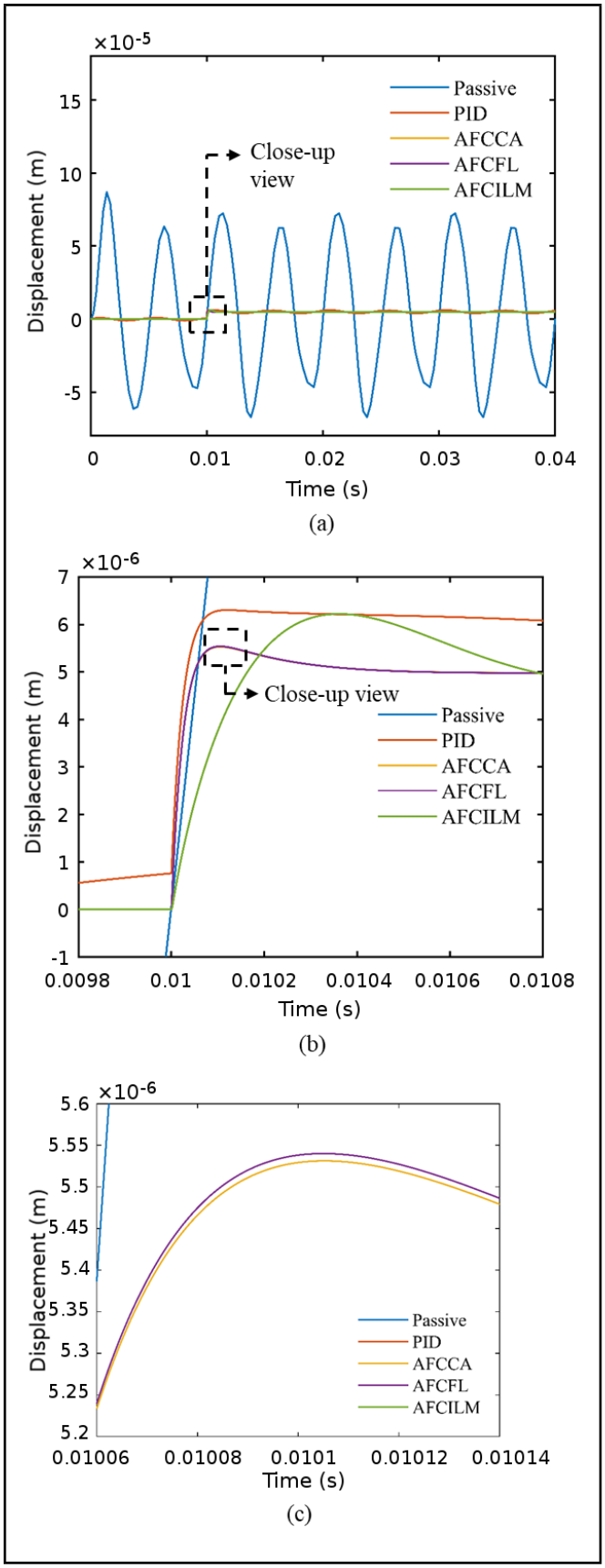

Figure 12. (a) Overall, (b) first level and (c) second level close-up views of output displacement of step input with internal and external disturbance A.

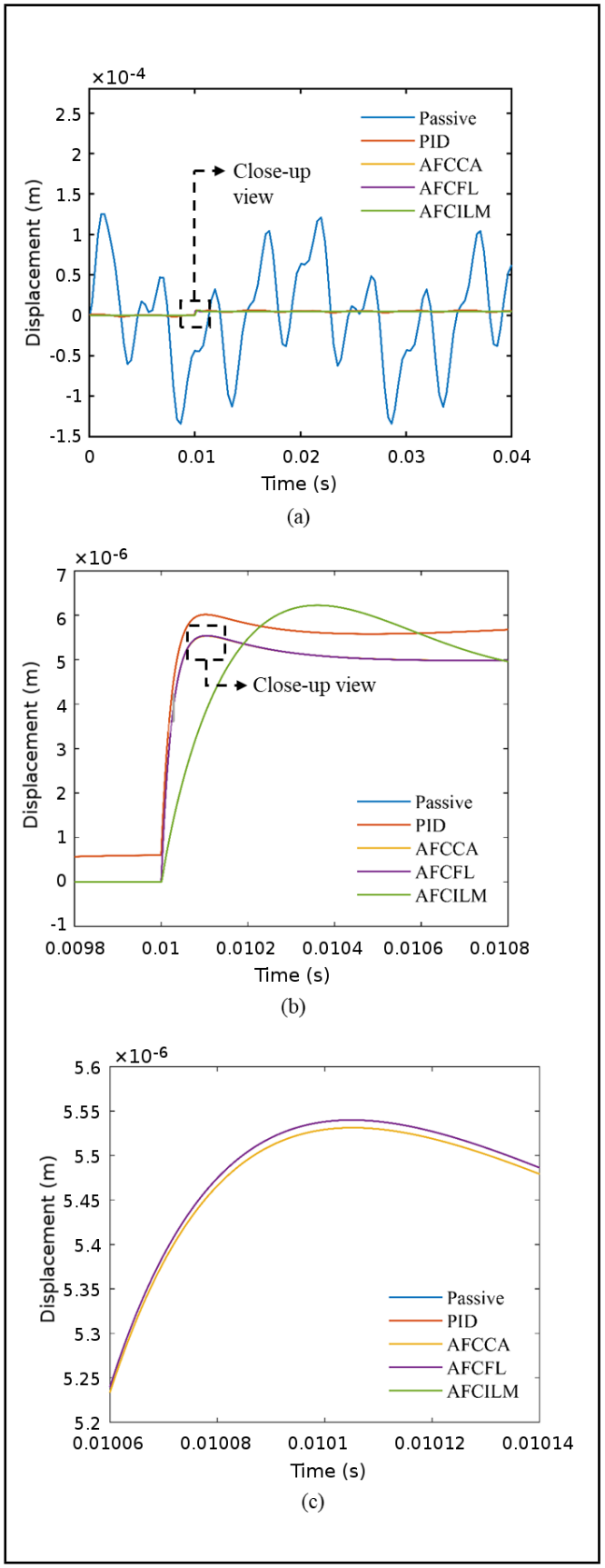

Figure 13. (a) Overall, (b) first level and (c) second level close-up views of output displacement of step input with internal and external disturbance B.

Table 6. Comparison between AFC schemes.

Parameters	Type of AFC schemes		
	PID-AFCCA	PID-AFCFL	PID-AFCILM
Optimum estimated mass value M^*, kg	0.04	0.0403	0.04
Displacement peak value during tuning of controller, 10^{-6} m	5.50	5.53	6.00
Step input with disturbances A & B, 10^{-6} m	5.53	5.54	6.33

As a future recommendation, the piezoelectric actuator nonlinearity such as force saturation can be adapted to the model to reflect an actual power tool application.

4. CONCLUSIONS

In this study, the attenuation of vibrations for the suspended handle model generated from power tools using different AFC intelligent tuning methods (i.e., CA, FL and ILM) were investigated. Two types of disturbances (i.e. internal and external) are introduced to the system. The estimated disturbance force from the AFC scheme is used to counter the disturbances and challenged the robustness of the AVC system. Based on the results, it can be seen that the passive and AVC with PID controller systems are affected by the external disturbances that been introduced to the system. Meanwhile, all the AFC schemes prove to be effective even under the influence of various disturbances and conditions, which prove the robustness of the controller. For the overall performances using the step input signal, the AFCCA scheme exhibits an upper hand over the other schemes as it demonstrates the best response with the lowest overshoot, fastest rise and settling times for AVC system.

ACKNOWLEDGEMENTS

The authors would like to acknowledge Universiti Sains Malaysia and Kementerian Pengajian Tinggi Malaysia for funding this work through the RUI Grant 1001/PMEKANIK/8014129 and FRGS Grant 203/PMEKANIK/6071370.

REFERENCES

[1] Mailah, M., and Rahim, N.I.A. Intelligent active force control of a robot arm using fuzzy logic, *Proceedings. Intelligent Systems and Technologies for the New Millennium*, Kuala Lumpur, 291–296, (2000). https://dx.doi.org/10.1109/TENCON.2000.888750

[2] Gurram, R., Rakheja, S., and J. Gouw, G. Vibration transmission characteristics of the human hand-arm and gloves, *International Journal of Industrial Ergonomics*, **13**(3), 217–234, (1994). https://dx.doi.org/10.1016/0169-8141(94)90069-8

[3] Pyykko, I., A. Farkkila, M., Toivanen, J., Korhonen, O., and Hyvärinen, J. Transmission of vibration in the hand arm system with special reference to changes in compression force and acceleration, *Scandinavian Journal of Work, Environment and Health*, **2**(2), 87–95, (1976). https://dx.doi.org/10.5271/sjweh.2820

[4] Xu, X.S., Dong, R.G., Welcome, D.E., Warren, C., McDowell, T.W., and Wu, J.Z. Vibrations transmitted from human hands to upper arm, shoulder, back, neck, and head, *International Journal of Industrial Ergonomics*, **62**, 1–12, (2017). https://dx.doi.org/10.1016/j.ergon.2016.07.001

[5] Reynolds, D.D., and Soedel, W. Dynamic response of the hand-arm system to a sinusoidal input, *Journal of Sound and Vibration*, **21**(3), 339–353, (1972). https://dx.doi.org/10.1016/0022-460X(72)90818-8

[6] Romaiguère, P., Vedel, J.P., and Pagni, S. Effects of tonic vibration reflex on motor unit recruitment in human wrist extensor muscles, *Brain Research*, **602**(1), 32–40, (1993). https://dx.doi.org/10.1016/0006-8993(93)90237-H

[7] Rohmert, W., Wos, H., Norlander, S., and Helbig, R. Effects of vibration on arm and shoulder muscles in three body postures, *European Journal of Applied Physiology and Occupational Physiology*, **59**(4), 243–248, (1989). https://dx.doi.org/10.1007/BF02388323

[8] Vijayan, V., Karthikeyan, T., Udayakumar, M., and Chellamuthu, K. Passive vibration isolation by compliant mechanism using topology optimization with building blocks, *International Journal of Acoustics and Vibration*, **8**(13), 1522–1530, (2014). https://dx.doi.org/10.19026/RJASET.8.1130

[9] Behrens, S., Fleming, A.J., and Moheimani, S.O.R. Passive vibration control via electromagnetic shunt damping, *IEEE/ASME Transactions on Mechatronics*, **10**(1), 118–122, (2005). https://dx.doi.org/10.1109/TMECH.2004.835341

[10] Abdelrahman, W.G., Al-Garni, A.Z., Abdelmaksoud, S.I., and Abdallah, A. Effect of piezoelectric patch size and material on active vibration control of wind turbine blades, *Journal of Vibrational Engineering and Technologies*, **6**(2), 155–161, (2018). https://dx.doi.org/10.1007/s42417-018-0020-9

[11] Martins, L.A., Lara-Molina, F.A., Koroishi, E.H., and Cavalini, A.A. Optimal design of a dynamic vibration absorber with uncertainties, *Journal of Vibrational Engineering and Technologies*, **8**(1), 133–140, (2020). https://dx.doi.org/10.1007/s42417-019-00084-6

[12] Meurers, T., and Veres, S.M. Iterative design for vibration attenuation. *International Journal of Acoustics and Vibration*, **32**(1), 79–83, (2000). https://dx.doi.org/10.20855/ijav.1999.4.235

[13] Nor, K.A.M., Muthalif, A.G.A., and Wahid, A.N. Optimization in active vibration control: virtual experimentation using COMSOL multiphysics - MATLAB integration, *Proceedings - International Conference on Intelligent Systems, Modelling and Simulation*, Kuala Lumpur, 385–389, (2015). https://dx.doi.org/10.1109/ISMS.2014.71

[14] Messer, M.H.E. Parametric excitation of vibrations in printing machines, *International Journal of Acoustics and Vibrations*, **22**(4), 448–455, (2017). https://dx.doi.org/10.20855/ijav.2017.22.4490

[15] Skogestad, S. Probably the best simple PID tuning rules in the world, *Journal of Process Control*, 1–27 (2001).

[16] Carbajal, F.B., Olvera, R.T., Garcia, I.L., Gonzalez, A.V., Caro, J.C.R., and Avila, J.L.H. Extended PI feedback tracking control for synchronous motors, *International Journal of Control, Automation and Systems*, **17**(6), 1346–1358, (2019). https://dx.doi.org/10.1007/s12555-018-0312-6

[17] Carbajal, F.B., Contreras, A.F., Avila, J.L.H., Tapia, O.O., Sotelo, D., and Carlos, S. Dynamic output feedback control for desired motion tracking on synchronous motors, *International Transactions on Electrical Energy Systems*, **30**(3), 1–18, (2020). https://dx.doi.org/10.1002/2050-7038.12260

[18] Jovanović, M.M., Simonović, A.M., Zorić, N.D., Lukić, N.S., Stupar, S.N., and Ilić, S.S. Experimental studies on active vibration control of a smart composite beam using a PID controller, *Smart Materials and Structures*, **22**(11), (2013). https://dx.doi.org/10.1088/0964-1726/22/11/115038

[19] Zhang, S., Schmidt, R., and Qin, X. Active vibration control of piezoelectric bonded smart structures using PID algorithm, *Chinese Journal of Aeronautics*, **28**(1), 305–313, (2015). https://dx.doi.org/10.1016/j.cja.2014.12.005

[20] Elsrogy, W.M., Fkirin, M.A., and Hassan, M.A.M. Speed control of DC motor using PID controller based on artificial intelligence techniques, *International Conference on Control, Decision and Information Technologies*, Hammamet, 196–201, (2013). https://dx.doi.org/10.1109/CoDIT.2013.6689543

[21] Khan, L., Qamar, S., and Khan, U. Adaptive PID control scheme for full car suspension control, *Journal of the Chinese Institute of Engineers*, **39**(2), 169–185, (2016). https://dx.doi.org/10.1080/02533839.2015.1091427

[22] Kada, B., and Ghazzawi, Y. Robust PID controller design for an UAV flight control system, *Proceedings of the World Congress on Engineering and Computer Science*, San Francisco, 1–6, (2011).

[23] Mailah, M., Hewit, J.R., Meeran, and S., Rhewit. Active force control applied to a rigid robot arm, *Jurnal Mekanikal*, **2**(2), 52–68 (1996).

[24] Kwek, L.C., Wong, E.K., Loo, C.K., and Rao, M.V.C. Application of active force control and iterative learning in a 5-link biped robot, *Journal of Intelligent and Robotic Systems: Theory and Applications*, **37**(2), 143–162, (2003). https://dx.doi.org/10.1023/A:1024187206507

[25] Rao, M.V.C., and Prahlad, V. A tunable fuzzy logic controller for vehicle-active suspension systems, *Fuzzy Sets and Systems*, **85** (1), 11–21, (1997). https://dx.doi.org/10.1016/0165-0114(95)00369-X

[26] Holou, N.A., Lahdhiri, T., Joo, D.S., Weaver, J., and Abbas, F.A. Sliding mode neural network inference fuzzy logic controller of nonlinear active suspension system, *IEEE Transactions on Fuzzy Systems*, **10**(2), 234–246, (1999). https://dx.doi.org/10.1109/91.995124

[27] Dehkordi, S.M.H., Bakar, A.R.A., Mailah, M. Reducing friction-induced vibration using intelligent active force control (AFC) with piezoelectric actuators, *Sadhana - Academy Proceedings in Engineering Sciences*, **37**(6), 637–655, (2012). https://dx.doi.org/10.1007/s12046-012-0104-2

[28] Peng, H., Strathearn, R., and Ulsoy, A.G. A novel active suspension design technique - simulation and experimental results, *Proceedings of the American Control Conference*, Albuquerque, 709–713, (1997). https://dx.doi.org/10.1109/ACC.1997.611893

[29] Gohari, M., and Tahmasebi, M. Active off-road seat suspension system using intelligent active force control, *Journal of Low Frequency Noise Vibration and Active Control*, **34**(4), 475–490, (2015). https://dx.doi.org/10.1260/0263-0923.34.4.475

[30] Abdullah, S., Mailah, M., and Hing, C.T.H. Feedforward model based active force control of mobile manipulator using MATLAB and MD adams, *WSEAS Transactions on Systems*, **12**(6), 314–324 (2013).

[31] Mazlan, A.Z.A., and Ripin, Z.M. Active vibration control to attenuate hand-arm vibration from orbital sander: A mathematical model approach, *International Conference on Computer Science and Computational Mathematics*, Kedah, 264–268, (2015). https://dx.doi.org/10.17485/ijst/2015/v8i30/85942

[32] Hassan, M.F., Mailah, M., Junid, R., and Alang, N.A. Vibration suppression of a handheld tool using intelligent Active Force Control (AFC), *Proceedings of the World Congress on Engineering*, London, 1636–1641, (2010).

[33] Tomohide, N., Arimoto, S., and Wada, K. A learning control method for coordination of multiple manipulators holding a geometrically constrained object, *Advanced Robotics*, **13**(2), 139–152, (1998). https://dx.doi.org/10.1163/156855399X00180

[34] Jian, Y., Huang, D., Liu, J., and Min, D. High-Precision tracking of piezoelectric actuator using iterative learning control and direct inverse compensation of hysteresis, *IEEE Transactions on Industrial Electronics*, **66**(1), 368–377, (2019). https://dx.doi.org/10.1109/TIE.2018.2826450

[35] Xu, J.X., Huang, D., Venkataramanan, V., and Huynh, T.C.T. Extreme precise motion tracking of piezoelectric positioning stage using sampled-data iterative learning control, *IEEE Transactions on Control Systems Technology*, **21**(4), 1432–1439, (2013). https://dx.doi.org/10.1109/TCST.2012.2201718

[36] Huang, R., Cheng, H., Chen, Q., Tran, H.T., and Lin, X. Interactive learning for sensitivity factors of a human-powered augmentation lower exoskeleton, *IEEE International Conference on Intelligent Robots and Systems*, Hamburg, 6409–6415, (2015). https://dx.doi.org/10.1109/IROS.2015.7354293

[37] Zhang, S., Schmidt, R., and Qin, X. Active vibration control of piezoelectric bonded smart structures using PID algorithm, *Chinese Journal of Aeronautics*, **28**(1), 305–313 (2015). https://dx.doi.org/10.1016/j.cja.2014.12.005

[38] Changhai, R., and Lining, S. Hysteresis and creep compensation for piezoelectric actuator in open-loop operation, *Sensors and Actuators A: Physical*, **122**(1), 124–130, (2005). https://dx.doi.org/10.1016/j.sna.2005.03.056

[39] Zhang, A.G., Yang, T.J., Du, J.T., Lv, P., and Li, X.G. Finite element analysis of piezoelectric materials, *Advanced Materials Research*, **860**, 872–875, (2014). https://dx.doi.org/10.1016/j.proeng.2012.09.528

[40] Mazlan, A.Z.A., and Jamaludin, H. Performance comparison of the PID-AFCCA and PID- AFCFL controllers in reducing the vibration of the suspended handle, *International Conference on Control, Mechatronics and Automation*, Tokyo, 105–110, (2018). https://dx.doi.org/10.1145/3284516.3284524

[41] Purnomo, S.D., Anom Besar, A.R., and Zaqiatud, D. Design and static analysis of airlesstyre to reduce deformation, *IOP Conference Series: Material Science and Engineering*, **36**, 10–12, (2012). https://dx.doi.org/10.1088/1757-899X/197/1/012042

[42] Singh, M., and Chandra, A. Application of adaptive network-based fuzzy inference system for sensorless control of PMSG-based wind turbine with nonlinear-load-compensation capabilities, *IEEE Transactions on Power Electronics*, **26**(1), 165–175, (2011). https://dx.doi.org/10.1109/TPEL.2010.2054113

[43] Wei, J.J., Qiu, Z.C., Han, J. Da, and Wang, Y.C. Experimental comparison research on active vibration control for flexible piezoelectric manipulator using fuzzy controller, *Journal of Intelligent and Robotic Systems: Theory and Applications*, **59**(1), 31–56, (2010). https://dx.doi.org/10.1007/s10846-009-9390-2

[44] Mailah, M. Intelligent active force control of a rigid robot arm using neural network and iterative learning algorithms, *Jurnal Mekanikal*, **13**, 50–63, (2002). https://dx.doi.org/10.11113/jt.v35.594

[45] Ahn, K.K., Truong, D.Q., Thanh, T.Q., and Lee, B.R. Online self-tuning fuzzy proportional-integral-derivative control for hydraulic load simulator, *Proceedings of the Institution of Mechanical Engineers. Part I: Journal of Systems and Control Engineering*, **222**(2), 81–95, (2008). https://dx.doi.org/10.1243/09596518JSCE484

[46] Toan, T.Q., Sorokin, A.A., and Trang, V.T.H. Fuzzy system for controlling queue size of packets in telecommunication nodes, *Moscow Workshop on Electronic and Networking Technologies*, Moskovskaya, 1–6, (2018). https://dx.doi.org/10.1109/MWENT.2018.8337252

[47] Ahlawat, A.S., and Ramaswamy, A. Multiobjective optimal structural vibration control using fuzzy logic control system, *Journal of Structural Engineering*, **27**(11), 1330–1337, (2001). https://dx.doi.org/10.1061/(ASCE)0733-9445(2001)127:11(1330)

[48] Lin, C.J., and Lin, P.T. Tracking control of a biaxial piezo-actuated positioning stage using generalized Duhem model, *Computers and Mathematics with Applications*, **64**(5), 766–787, (2012). https://dx.doi.org/10.1016/j.camwa.2011.12.015

[49] Mazlan, A.Z.A., and Ripin, Z.M. The effective frequency range of an active suspended handle based on the saturation effects of a piezo stack actuator, *Journal of Vibration and Control*, **23**(5), 752–769, (2017). https://dx.doi.org/10.1177/1077546315585218

[50] Inoue, T., Liu, J., Ishida, Y., and Yoshimura, Y. Vibration control and unbalance estimation of a nonlinear rotor system using disturbance observer, *Journal of Vibration and Acoustics*, **131**(3), (2009). https://dx.doi.org/10.1115/1.3085886

[51] Tang, L., and Yang, Y. A multiple-degree-of-freedom piezoelectric energy harvesting model, *Journal of Intelligent Material Systems and Structures*, **23**(14), 1631–1647, (2012). https://dx.doi.org/10.1177/1045389X12449920

[52] Xiao, H., Wang, X., and John, S. A multi-degree of freedom piezoelectric vibration energy harvester with piezoelectric elements inserted between two nearby oscillators, *Mechanical Systems and Signal Processing*, **68**, 138–154, (2016). https://dx.doi.org/10.1016/j.ymssp.2015.07.001

[53] Man, G.K.I., H, B.G., and Gosine, R.G. Time-domain based design and analysis of new PID tuning rules, *IEE Proceedings - Control Theory and Applications*, **148**(3), 251–261, (2001). https://dx.doi.org/10.1049/ip-cta:20010464

[54] Tang, K.S., Man, K.F., Chen, G., and Kwong, S. An optimal fuzzy PID controller, *IEEE Transactions on Industrial Electronics*, **48**(4), 757–765, (2001). https://dx.doi.org/10.1109/41.937407

[55] Mazlan, A.Z.A., Ripin, Z.M, Ali, W.M.A.W.M. Active vibration control using PID-AFC controller of the piezo stack actuator with consideration to hysteresis and saturation effects, *International Congress on Sound and Vibration*, London, 1-8, (2017).